A kinetics study of the methomyl electrochemical degradation in the chloride containing solutions

CrossMark

Branimir N. Grgur*, Dušan Ž. Mijin

Faculty of Technology and Metallurgy, University of Belgrade, Karnegijeva 4, 11020 Belgrade, Serbia

ARTICLE INFO

ABSTRACT

The kinetics of the electrochemical degradation of methomyl has been study by the means of electrochemical techniques, UV–vis spectrophotometry, HPLC, and HPLC–ESI-MS in the sodium chloride containing solution. Degradation kinetics has been investigated on the DSA Ti/RuO$_2$ electrode in mainly 2 g dm^{-3} sodium chloride solution, applying the currents in the range of 10–90 mA and methomyl concentration from 0.05 to 0.5 mM. It has been suggested that methomyl degradation initially follows the pseudo zero-order Langmuir–Hinshelwood reaction kinetics, and mixed homogeneous and heterogeneous pseudo first-order reaction during prolonged electrolysis.

1. Introduction

Contamination of soil, surface and ground waters *etc.* with different classes of pesticides, under extensive agricultural activities become a huge environmental and health risk due to their high toxicity. The consequent restrictions imposed by new legislation require effective initiatives for pollution reduction and control [1]. Under certain environmental conditions degradation of some pesticide could occur *via* hydrolysis, photolysis, or oxidation with some metal ions present in the soil [2]. Very important issue in pesticide contamination control is preventing waste water from agricultural or industrial activities. The major sources of pollution by pesticides are waste water from agricultural industries, pesticides formulating and manufacturing plants. Waste water from those sources may contain pesticides at levels of few μg dm^{-3} to as high as several hundred mg dm^{-3}. The main characteristics of this waste water are its extreme toxicity, low volume and well-defined location. Suitable treatment is therefore required to prevent it, which is easier than cleaning up the environment afterwards. Such point sources of pollution may be ideally treated in small-scale treatment units [3]. Among different physico-chemical processes, advanced oxidation processes (AOPs) have been proposed as an alternative for the treatment of this type of wastewater. Although different reacting systems are used, they are all characterized by the same chemical feature, production of OH radicals (OH*). These radicals are extraordinarily reactive with oxidation potential of 2.8 V and attack most organic molecules [4–7]. Free radicals in AOPs, may be produced by photochemical and non-photochemicals procedures [4–7]. Today, few AOPs dominate: heterogeneous photocatalysis (mainly TiO$_2$/UV), homogeneous photocatalysis (Fenton and Fenton-like processes) and electrochemical oxidation on high oxygen overvoltage anodes, for example Pb/PbO$_2$, Ti/SnO$_2$, and boron doped diamond electrode (BDD) [4–9]. Even the AOPs have many advantages, due to the specific requirements like better efficiency in acidic solution, addition of the catalyst, reaction control or relatively high energy consumption could not be used in all occasions [4].

Little attempt has been made in the investigation of pesticide degradation with the active chlorine species (Cl$_2$ + HOCl + OCl$^-$) which can be easily produced electrochemically from dilute chloride containing solutions and is widely used for other pollutant decontaminations [10–12]. For example, Vlyssides et al. [13] investigated degradation of four commercial phosphorothioate obsolete pesticides stocks in the laboratory scale pilot plant using Ti/Pt anode with addition of 4% NaCl. They found considerably improvement of COD/BOD$_5$ ratio after electrolysis for all four pesticides examined and concluded that electrochemical oxidation could be used as a pretreatment method of the pesticides detoxification. Muff et al. [14] investigated degradation of several organophosphoric pesticide polluted in natural water with salinity of ∼0.7%. Using the Ti/Pt$_{90}$Ir$_{10}$ anode in tubular flow cell, measuring the COD showed that the overall oxidation followed first-order
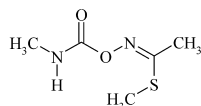
Fig. 1. Methomyl structure of the most common *cis*-isomer.

kinetics in the current densities range of 310–1131 mA cm^{-2}. The COD removal rate increased by increased current density and to a minor extent by increased salinity. The degradation of the subjected organics was suggested to be caused by indirect oxidation by the hypochlorous/hypochlorite pair as the main oxidizing agent, produced by the anodic oxidation of chloride. Their study has showed that electrochemical chloride mediated indirect oxidation is a relevant, neat and possible solution for the remediation of organophosphoric pesticide polluted natural water.

Several reasons can be wielded to explain this little attention given to the study of pesticide degradation with active chlorine, but all seems to indicate that this lack of attention is the risk to form products of pesticides even more toxic than the parent compound. The most research has been done with the goal to investigate mechanism of the pesticide and other pollutants degradation under the simulated chlorinated community water systems [15,16]. For example, four sulfur-containing *s*-triazines were found to degrade in the presence of free chlorine [17,18]. The proposed reaction center and transformation pathway for each *s*-triazine was oxidation of the sulfur resulting in the formation of sulfoxide and sulfone degradation products. Some carbamate pesticides have been shown to react with free chlorine while other members of this pesticide class were found to be stable in chlorinated water. For example, carbaryl does not react with free chlorine, but aldicarb, methomyl, and thiobencarb do exhibit significant reactivity [19–21]. The sulfoxide degradate of thiobencarb–produced by reaction with free chlorine was found to be mutagenic [21]. However, the by-products of aldicarb were found to be less toxic than the parent [20]. These findings demonstrate that active chlorine reactivity with different members in a specific class of pesticides can vary significantly due to chemical structure variations.

In that manner the methomyl as a typical thiocarbamate pesticide has been chosen as a model system to investigate kinetics of degradation with electrochemically formed active chlorine as an alternative to AOPs in some occasion. Such systems could be used for *in situ* degradation, for example the water from washing pesticide bottles, rinse water polluted by pesticide formulations from containers used in greenhouses or aircraft sprayers, from the manufacturing industry, or from washing fruits and vegetable prior to marketing, *etc.*

Methomyl (S-methyl N-[(methylcarbamoyl)oxy]thioacetimidate), which structural formula is shown in Fig. 1, is a typical pesticides which belongs to the family of thiocarbamate and is widely used as a broad spectrum insecticide [22]. It is a very toxic and hazardous compound. Due to high solubility in water (57.9 g dm^{-3} at 25 °C) [23] methomyl has been detected in surface and ground waters across Europe and America, even after a long period of use [24]. Methomyl is relatively stable to hydrolysis under neutral and acidic conditions. It has a hydrolysis DT$_{50}$ value of 36 days at pH 9.0 and temperature of 25 °C. Methomyl is also not easily biodegradable [25], and is a product of some pesticide degradation, for example thiodicarb [26].

Methomyl have been subjected to different processes in order of removal from waste waters and environment. The degradation of methomyl by direct photolysis represents a minor degradation pathway [27]. Tamimi et al. [27] confirmed that direct photolysis occurs, but observed <4% degradation following 45 min of UV irradiation. Phocatalysis using 25 cm^{-3} of methomyl solution (0.123 mM) and 62.5 mg of Degussa-P25 TiO$_2$ was the more

efficient degradation pathway for methomyl degradation. Among different unknown reaction product, methomyl oxime was produced, with additional breakdown products including acetonitrile, acetamide, acetic acid, glycolic acid, oxalic acid, formic acid, and CO$_2$. Tamimi et al. [28] also conducted various photocatalytic experiments and found that photo-Fenton and Fenton reactions more efficiently degraded methomyl (100% and 86.1%, respectively), than direct photolysis and UV + H$_2$O$_2$-catalyzed reactions (<4% and 60%, respectively). Under their experimental conditions for photo-Fenton first-order rate kinetics constant $k = 0.175$ min^{-1} and half-life of $\sim$4 min was obtained. The solar driven homogeneous photo-Fenton and heterogeneous TiO$_2$ processes for methomyl detoxification in water have been evaluated by Malato et al. [4,29,30]. According to TOC removal, the photo-Fenton process was more efficient in degradation of 50 mg dm^{-3} of methomyl than the TiO$_2$ process. The both processes were capable of mineralizing more than 90% of the pesticide. Barakat et al. [31] improved the TiO$_2$ driven photolysis using the small size CdSO$_4$-doped TiO$_2$ nanoparticles. A 2000 mg dm^{-3} methomyl aqueous solution can be completely treated within 1 h at room temperature under sunlight irradiation. The removal capacity reaches to 1000 mg per gram photocatalyst. It was also reported that methomyl can be degraded by photo-Fenton reaction using supported iron catalysts, such as Fe-ZSM-5 zeolite and AlFe-pillared montmorillonite [32–34]. Mico et al. [35,36] found that oxidation *via* ozonation (10.5 mg dm^{-3} O$_3$ at pH 4.5) occurs more rapidly than the photo-Fenton reaction, with complete degradation occurring within 60 min, and that high salinity enhanced the methomyl photo-Fenton oxidation.

Oxidation of methomyl using free chlorine, chlorinated water, monochloramine, chlorine dioxide, hydrogen peroxide, ozone, and permanganate was also reported [37].

Miles and Oshiro [38] have reported that when methomyl was degraded in simulated chlorinated drinking water (1 μM active chlorine/0.l μM methomyl ratio), methomyl sulfoxide and N-chloromethomyl were the major products before degradation to acetic acid, methanesulfonic acid and dichloromethylamine. The methomyl breakdown varies; changes in pH between 7.6 and 8.9 produced half-lives differing by 30-fold (0.4–12 min), concluding that HOCl was the major oxidizing species. At pH ranges from 7.5 to 8.2 reactions follows the pseudo first-order rate with $k \sim 1.8$ min^{-1}. At near neutral pH mainly sulfoxidation occurs, whereas N-chlorination predominates at higher pH. Reaction rate with free chlorine was 1000-fold faster than with chloramines.

To our knowledge, only few references were found dealing with electrochemical degradation of methomyl [39–41]. In the first, a gold electrode was used for the electrochemical detection of analytical methomyl in a neutral electrolyte (0.05 M NaHCO$_3$) using linear sweep cyclic voltammetry. By cycling the potential in the range from −1300 mV *vs.* SCE to 1300 mV *vs* for 150 min, only 6% degradation of methomyl was achieved [39]. In the second, electrogenerated Fenton's reagent was used for Lannate 20 L (methomyl based pesticide) degradation [40,41]. Different Fenton's reagent, which was generated *in situ* electrochemically, lead to the formation of hydroxyl radicals. Formed hydroxyl radicals caused degradation of methomyl with rate in the turn of Fe^{3+} > Co^{2+} > Ag$^+$ > Cu^{2+}. Analyzing the TOC removal ratio for electro-Fenton and photo-Fenton processes Oturan et al. [42] demonstrated that the photo-Fenton process was more efficient than the electro-Fenton process in short treatment times. But the cost calculations based on reagent and electrical energy consumption has shown that the electro-Fenton process costs almost 4 times less than the photo-Fenton process.

In this paper we want to report a study of the electrochemical degradation of methomyl in the sodium chloride containing solutions. Kinetic study as well as the influence of the basic operational parameters such as applied current, hydrodynamic conditions,

initial concentration of methomyl and NaCl on the degradation mechanism was investigated, as guidance for the further more comprehensive studies.

2. Experimental

2.1. Materials

Analytical standard of methomyl (99.8%) was received as a present from DuPont de Nemours, USA. Sodium chloride was p.a. grade (Merck). Acetonitrile used for HPLC analysis was HPLC grade and was provided by J.T. Baker. All solutions were prepared with Millipore Waters deionized water (18.2 MΩ/cm at 25 °C) and were prepared prior to use.

2.2. Electrochemical measurements

Polarization and cyclic voltammetry measurements were performed in three compartment electrochemical glass cell. DSA Ti/RuO$_2$ anode with 1 mg cm^{-2} of the RuO$_2$, or stainless steel series 304 cathode (for the hydrogen evolution experiments) with the surface area of 2 cm^2 was used as the working electrodes. The saturated calomel electrode as a reference electrode, and platinum foil as a counter electrode was used. Potenciostat/galvanostat PAR 273 A controlled by a computer through a GPBI PC2A interface was used in all measurements.

2.3. Electrochemical degradation

The electrochemical degradation process was investigated in cylindrical glass electrochemical cell with an electrolyte volume of 500 cm^3. The electrolyte was prepared from deionized water, NaCl and methomyl. As anode 5 cm^2 DSA Ti/RuO$_2$ obtained by thermal decomposition of RuCl$_3$ in 2-propanol at 400 °C on the Ti plate, with 1 mg cm^{-2} of RuO$_2$ loading was used, while cathode was 10 cm^2 plate made from austenite 18Cr/8Ni stainless steel series 304. Electrode, with the gap of 3 mm, was immersed at the top of the electrolyte. Mixing of the electrolyte was accomplished by magnetic stirrer. During the electrolysis at certain times 3 cm^3 of the solution was taken with micropipette and UV–vis spectra was instantly recorded. The concentration of methomyl was followed by measuring the absorption of the solution at 233.8 nm, using UV–vis Shimadzu model 1700 spectrophotometer.

2.4. HPLC analysis

For HPLC determination, all samples were filtered through 0.45 μm syringe filters and were analyzed at 234 nm and at ambient temperature (25 °C) on a SpectraSYSTEM P4000 liquid chromatograph with a SpectraSYSTEM UV1000 detector, equipped with a reversed phase column type Zorbax SB C8 (150 mm × 4.6 mm i.d., 5 μm particle size). The mobile phase (flow rate 1.0 mL min^{-1}) was a mixture of acetonitrile and water (30:70, v/v), 0.1% formic acid solution. Sample injection volume was 20 μL.

2.5. LC–MS analysis

All samples were filtered through 0.45 μm syringe filters and were analyzed by LC–MS technique (HPLC Agilent 1200 Series, Agilent Technologies equipped with degasser, autosampler, column Zorbax Eclipse XDB C8 (150 mm × 4.6 mm i.d., 5 μm particle size) and DAD detector coupled with 6210 Time-of-Flight LC/MS systems, Agilent Technologies) was used. The mobile phase consisted of solvent A (0.2% formic acid solution in water) and solvent B (acetonitrile). An isocratic method was used: 0–15 min 30% B at flow
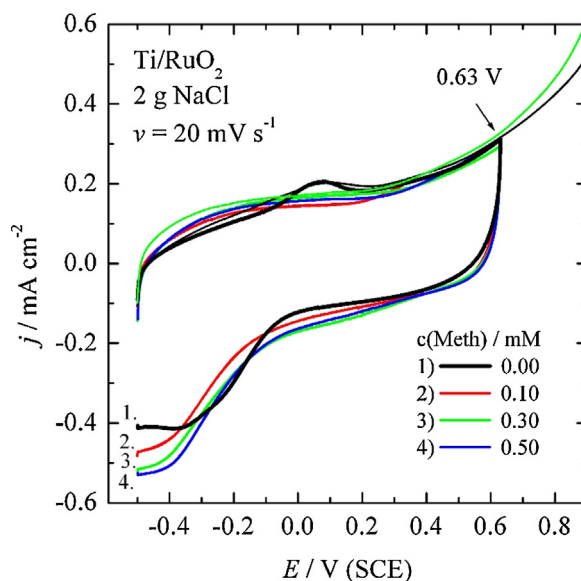

Fig. 2. Cyclic voltammogram of the Ti/RuO$_2$ electrode in solution with different methomyl concentration.

rate 0.4 cm^3 min^{-1}. The injection volume was 10 μL and the column temperature was maintained at 25 °C. The chromatograms were monitored at 190–450 nm using DAD detector.

The positively charged molecular ions were obtained with electrospray ionization (ESI) at atmospheric pressure: the eluated compounds were mixed with nitrogen in the heated nebulizing interface, and polarity was tuned to positive with the following ESI parameters: capillary voltage 3.0 kV, gas temperature 350 °C, drying gas flow rate 12 dm^3/min, nebulizer pressure 45 psig (310.26 Pa), and fragmentor voltage 70 V. Mass spectra were acquired over an m/z range of 100–1500. A personal computer system running MassHunter Workstation software was used for data acquisition and processing. Bruto molecular formula of components was calculated using molecular feature extractor on the basis of precisely determined molar mass.

3. Results and discussion

3.1. Electrochemical polarization investigation

Cyclic voltammograms of Ti/RuO$_2$ electrode for different methomyl concentration is shown in Fig. 2. Without methomyl in the solution anodic part of the voltammogram is characterized by a broad peak in the potential range of −0.1 to 0.15 V, which corresponds to the RuO$_x$ surface redox reaction. In the cathodic scan at the potentials below −0.05 V, oxygen reduction reaction occurred. When the methomyl was present in solution, the broad peak in anodic direction was completely suppressed, while the oxygen reduction reaction in the cathodic scan was accelerated, and starts at the potentials of ~0.4 V. It can be seen that limiting diffusion current density of oxygen reduction reaction increase with methomyl concentration. Considering such behavior, it could be proposed that methomyl is probably adsorbed on the electrode surface reducing the possibilities of the formation of higher ruthenium oxides. Desorption of the methomyl in the cathodic scan liberate Ru oxide sites with lower oxidation states which are probably more active for the oxygen reduction reaction than over oxidized states, like in the case of the platinum with adsorbed sulfur containing species [43]. Extending the anodic potential limits to 0.9 V some higher activity when methomyl is present in solution was observed at potentials as low as 0.63 V.
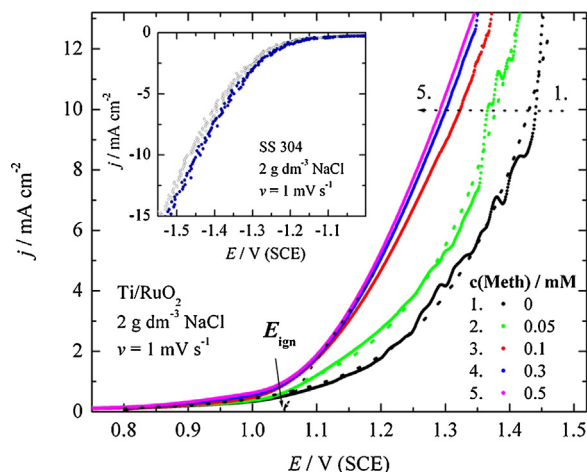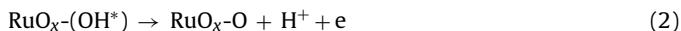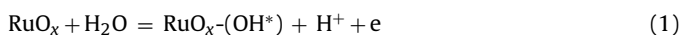
Fig. 3. Slow potentiodinamic polarization curves at Ti/RuO$_2$ electrode for different methomyl concentrations. Insert: Polarization curves of SS cathode in (○) 2 g dm^{-3} NaCl and in (●) 15 min pre-electrolyzed solution with Ti/RuO$_2$ at 10 mA cm^{-2}.
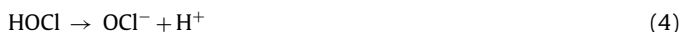

Fig. 4. Typical UV spectra changes of methomyl (c_0 = 0.1 mM) in 2 g dm^{-3} NaCl water solution during electrochemical degradation (I = 50 mA, ω = 250 rpm). Insert: Dependence of the relative methomyl concentration in 2 g dm^{-3} (●) NaCl; (▲) Na$_2$SO$_4$ and (○) pH over time.

Fig. 3 shows slow potentiodinamic polarization curves at Ti/RuO$_2$ electrode in the electrolyte of 2 g dm^{-3} NaCl without and for the different methomyl concentrations. For the polarization curves without and with 0.05 mM of the methomyl gas bubbling from the electrode surface was observed. For those two curves for the further analysis, NLSF was applied (shown as a dotted line). On the "active RuO$_2$ electrode" near neutral pH, gas evolution, most probably oxygen is a competitive reaction to the active chlorine formation through the following reactions [1]:

$$RuO_x + H_2O = RuO_x\text{-}(OH^*) + H^+ + e \tag{1}$$

$$RuO_x\text{-}(OH^*) \rightarrow RuO_x\text{-}O + H^+ + e \tag{2}$$

$$2RuO_x\text{-}O \rightarrow 2RuO_x + O_2 \tag{2a}$$

or

$$RuO_x\text{-}(OH^*) + Cl^- \rightarrow RuO_x\text{-}(HOCl^*) + e \tag{3}$$

$$RuO_x\text{-}(ClOH^*) \rightarrow RuO_x + HOCl \tag{3a}$$

followed by dissociation in solution:

$$HOCl \rightarrow OCl^- + H^+ \tag{4}$$

The current efficiency for the active chlorine production on Ti/RuO$_2$ in low concentrations of NaCl was estimate to be maximally 20% [44]. Increasing the methomyl concentration above 0.05 mM gas bubbling was not observed suggesting that reaction given by Eq. (2a) was reduced or practically eliminated. It is interesting to note that even some activities was observed at potentials more positive than 0.63 V (Fig. 2) significant oxidation starts at potentials above 1.05 V which could be assigned to "ignition" potential, E_{ign}. Increases of the methomyl concentrations increase the reaction rate. For example at the current density of 10 mA cm^{-2} for the methomyl concentration of 0 and 0.5 mM a potential shift of ~150 mV in negative direction was observed. In the insert of Fig. 3, cathodic polarization curves, without methomyl, on the stainless steel electrode in the initial solution and after 15 min of electrolysis with current density of 10 mA cm^{-2} on RuO$_2$ anode were shown. Small differences in the activity suggest that cathodic reduction of active chlorine could be practically neglected. The noticeable hydrogen evolution occurred at the potentials below −1.15 V.
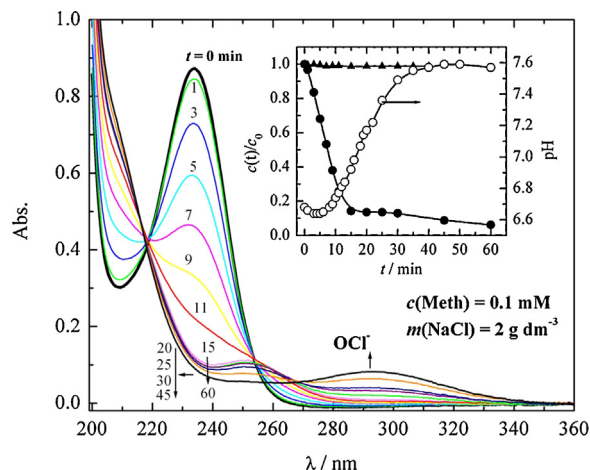
3.2. Electrochemical degradation in the batch reactor

3.2.1. UV spectra changes

The typical changes in the absorption spectra of solution containing 2 g dm^{-3} NaCl and 0.1 mM methomyl during the electrochemical degradation in the batch reactor for different reaction times are presented in Fig. 4. The methomyl shows a band with a maximum absorption at 233.8 nm. The decrease of the methomyl absorption peak during ~10 min actually indicates a fast degradation over time. After ~15 min, when ~ 90% of initial methomyl was degraded, the new absorption peak at 251–255 nm appears which slowly decrease during prolonged electrolysis. This new absorption peak could be connected with the existence of the reaction intermediates, which are degraded more slowly than methomyl, as also observed by TOC measurement during methomyl degradation by UV-irradiation in the presence of TiO$_2$ [27]. An increase of the absorption peak at 292 nm over time was observed, corresponding to the hypochlorite [45]. In addition, an isosbestic point was found in the UV spectra at 218 nm. As it can be seen from the insert in Fig. 4, the relative concentration of the methomyl practically linearly decreases during 15 min of electrolysis. The pH of the solution initially decreases, and after 6 min start slowly to increase, reaching the steady state value of ~7.6 after 35 min. At this pH value for the similar sodium chloride concentration an equimolar concentration of the hypochlorite and hypochlorous acid was formed [Fig. 1 in Ref. [16]]. Since in the absorption spectra increase at 236 nm (hypochlorous acid absorption maximum) [45], was not observed even after 60 min of the electrolysis, it could be proposed that this species is an electro active form. In the same insert of Fig. 4 the results obtained in solution containing 2 g dm^{-3} of Na$_2$SO$_4$ and 0.1 mM methomyl was shown, because of the possibilities that during anodic water oxidation could result in the formation of hydroxyl radicals which can easily oxidize the methomyl [1,11]. Under such conditions no activity was observed, so it could be concluded that hydroxyl radicals are not involved in the reaction mechanism, probably due to the fast formation of higher Ru oxides and oxygen evolution. One more important conclusion from this experiment is that methomyl was not cathodically reduced during the electrochemical degradation.

3.2.2. The influence of the electrolysis parameters
3.2.2.1. The influence of applied current.
In Fig. 5 the influence of applied current on methomyl degradation was shown. Initial linear dependence of the relative methomyl concentration over time
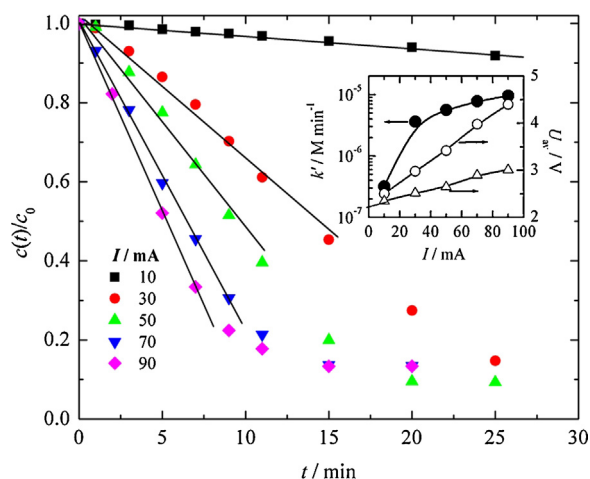
Fig. 5. Dependence of relative methomyl concentration ($c_0 = 0.1$ mM) over time for different applied current (marked in the figure) in a solution containing 2 g dm^{-3} NaCl, $\omega = 325$ rpm. Insert: the logarithmic plot of the (●) apparent zero-order reaction rate constant, (○) average and (△) Ohmic drop corrected electrolysis voltage for different current.

suggests pseudo zero-order reaction kinetics in respect to methomyl (see discussion in Section 3.4). In that case apparent zero-order reaction rate constant, k', can be calculated using the following equation:

$$\frac{c(t)}{c_0} = 1 - \frac{k'}{c_0}t \tag{5}$$

where $c(t)$ is actual, and c_0 initial methomyl concentration.

As it can be seen, with applied current of 10 mA ($j = 2$ mA cm^{-2}) reaction was very slow ($k' = 3.2 \times 10^{-7}$ M min^{-1}), but increasing the applied current the reaction rate increase as well. For the applied currents in the range of 30–90 mA apparent zero-order reaction rate constant increase from 3.6×10^{-6} to 9.5×10^{-6} M min^{-1} (see insert in Fig. 5). The increase of reaction rate with applied current could be attributed to the faster formation of electro active species, e.g. HOCl or OCl$^-$. Hence, higher current will be favorable for faster degradation, but 50 mA was chosen for the further studies as a compromise between the rate of the reaction and amenities of the experimental measurements.

Average electrolysis voltage, U_{av}, practically linearly increases with applied current from ~2.5 (3.0) V for 10 (30) mA to 4.4 V for 90 mA, as shown in the insert of Fig. 5. The structure of the electrolysis voltage can be given with following equation:

$$U = U_0 + \Sigma \left| \eta \right| + I\Sigma R \tag{6}$$

where U_0 represent differences of anodic and cathodic potentials at zero current (minimum decomposition voltage), I current, R sum of the Ohmic drops in the system and $|\eta|$ the absolute values of all anodic and cathodic overvoltages. Ohmic drop of the system could be approximately estimated taking into account that most of that part correspond to the solution resistivity:

$$R = \frac{l}{\kappa(\text{NaCl})A} \tag{7}$$

where $\kappa(\text{NaCl})$ is the specific conductivity of NaCl solution, $\kappa(2 \text{ g dm}^{-3} \text{ NaCl}) = 3.89$ mS cm^{-1}), l and A, are electrode distance and area, respectively. With the estimated solution resistivity of 15.4 Ω, the average electrolysis voltage was corrected and also shown in the insert of Fig. 5. Extrapolating the corrected average electrolysis voltage to zero current, U_0 of ~2.2 V was determined, which is practically identical to the differences of ignition (1.05 V) and noticeable hydrogen potentials (−1.15 V). The percentual structure of the electrolysis voltage for example at 50 mA
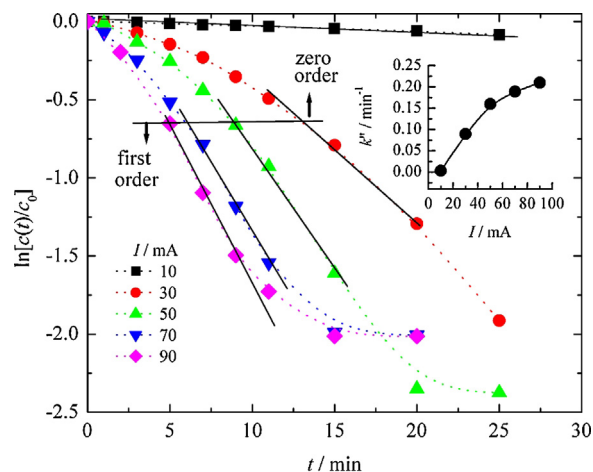
is, $U_{av} = 3.42$ V, IR (0.77 V) = 22.5%, U_0(2.2 V) = 64.3% and the rest of 13.2% or 0.45 V corresponds to anodic and cathodic overvoltages.

Since ~90% of 0.1 mM methomyl was degraded during 30 min, an average specific energy consumptions in the current range of 30–90 mA will be 2.8–12.2 kW h kg^{-1} of methomyl.

It was shown in Figs. 4 and 5 that the initial reaction rates follow zero-order kinetic. After certain times, the change from the zero to first-order kinetics was observed, as it can be seen in Fig. 6. Apparent first-order reaction rate constant, k'', can be calculated from the slope of the logarithm plot over time according to expression:

$$\ln \frac{c(t)}{c_0} = -k''t \tag{8}$$

Determined apparent first-order reaction rate constant, shown in the insert of Fig. 6, increase with current ranging from 3.3×10^{-3} to 0.21 min^{-1}. The transition time from zero to first-order kinetics corresponds to decrease in methomyl concentration of approximately 50%.

3.2.2.2. The influence of hydrodynamic rate. The influence of the solution mixing is shown in Fig. 7. Unusually, with increasing the stirring speed initial reaction rate decrease as it can be seen from the insert in Fig. 7, and becomes practically independent
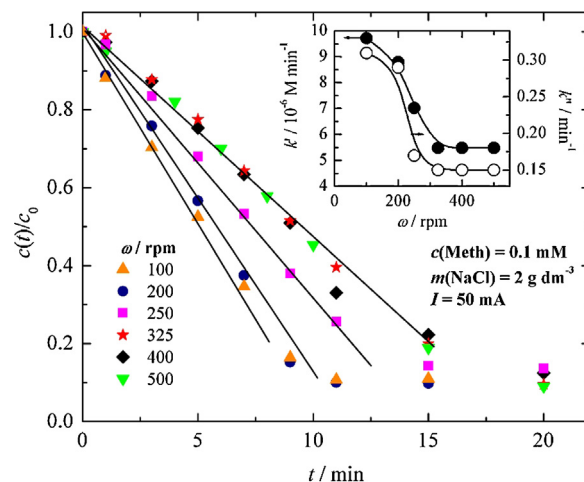

Fig. 6. The logarithmic plot of the relative methomyl concentration ($c_0 = 0.1$ mM) in a solution containing 2 g dm^{-3} NaCl for different applied current *versus* electrolysis time. Insert: Dependence of pseudo first-order reaction on applied current.

Fig. 7. Dependence of relative methomyl concentration ($c_0 = 0.1$ mM) over time for different stirring rate (marked in the figure). Insert: plot of the apparent (●) zero and (○) first-order reaction rate constant for different stirring rate.
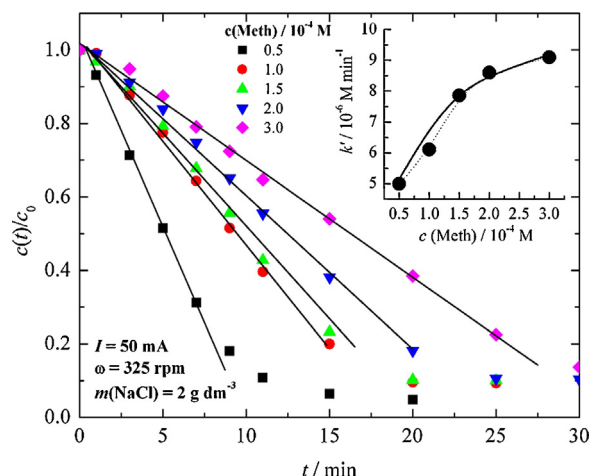
Fig. 8. Dependence of relative methomyl concentration over time for different initial methomyl concentration (marked in the figure). Insert: plot of the apparent zero-order reaction rate constant for different initial methomyl concentration, solid line: fit of Eq. (18) with $K = 17.9 \times 10^3$ M^{-1}, $k'_{sat} = 1.09 \times 10^{-5}$ M min^{-1}.
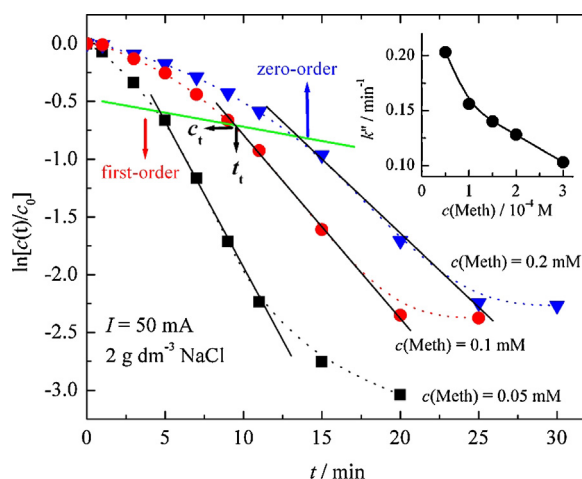

Fig. 9. The logarithmic plot of the relative concentration of 0.05, 0.1 and 0.2 mM methomyl in a solution containing 2 g dm^{-3} NaCl *versus* electrolysis time. Insert: Dependence of pseudo first-order reaction rate constant on methomyl concentration.

above ∼300 rpm. This behavior suggests that the reaction initially is probably not homogeneous, but maybe a heterogeneous surface reaction as discussed by Vargasa et al. [46] for the processes following the Langmuir–Hinshelwood mechanism. Namely, with the increases of the stirring rate, delicate balance between the rate of the diffusion and the adsorption of reacting species at the electrode surface and the rate of oxidation could be changed, provoking the decrease of reaction rate. By the same analysis for the first-order kinetics (figure not shown) using Eq. (8), the apparent first-order rate constant was also determined and shown in the insert of Fig. 7; for 100 and 200 rpm of ∼0.3 min^{-1}, for 250 rpm 0.17 min^{-1} and above reaching the limiting value of 0.15 min^{-1}.

3.2.2.3. The influence of the initial methomyl concentration. The influence of the initial methomyl concentration was investigated in the range of 0.05–0.3 mM and results are shown in Fig. 8. The required time for degradation increase with methomyl concentration, but taking into account Eq. (5), the apparent zero-order rate constant nonlinearly increase from 5×10^{-6} to 9×10^{-6} M min^{-1} as shown in the insert of Fig. 8. For the nominal studies performed, plotting pseudo zero-order reaction constants as a function of methomyl concentration, again hinted the possibility of an initial Langmuir–Hinshelwood type mechanism, with probable saturation of the surface sites with reacting species at methomyl concentration > 0.3 mM.

Following the analysis for the pseudo first-order reaction, graphical presentation of Eq. (8) for the methomyl concentration of 0.05, 0.1 and 0.2 mM is shown in Fig. 9. This kind of dependence was observed only after certain, transition times (t_t) when methomyl actual, transition concentration (c_t) falls below 50 to 60% of the initial one (%c_0). Estimated kinetics parameter for all investigated methomyl concentrations are summarized in Table 1.

3.2.2.4. The influence of the sodium chloride concentration. In the above experiments the concentration of NaCl was keep constant (0.2%), but considering the possible practical application, for example using sea or diluted sea water, wider range of NaCl concentration was also investigated.

Fig. 10 shows the dependence of relative methomyl concentration over time for different sodium chloride concentration, from which it can be seen that reaction rate increase with the increase of the sodium chloride concentration. This behavior could be connected with increase of current efficiency of the active chlorine species formation, and decrease of the rate of the oxygen evolution with increase in the sodium chloride concentration [10,47]. From the insert of Fig. 10 it could be seen that apparent zero-order reaction constant practically linearly increase from 6×10^{-6} to 18×10^{-6} M min^{-1} with an increase of the sodium chloride concentration from 2 to 20 g dm^{-3}. Increasing the NaCl concentration for ten times initial reaction rate increases only for three times.

For the further optimization, the average electrolysis voltage was measured and analyzed. Electrolysis voltage (shown in the insert of Fig. 10) decrease with sodium chloride concentration from ∼3.4 V for 2 g dm^{-3} to 2.2 V for 20 g dm^{-3}. Since κ(NaCl) pactically

Table 1
Evaluated kinetics parameters for pseudo first-order reaction for different initial methomyl concentration.

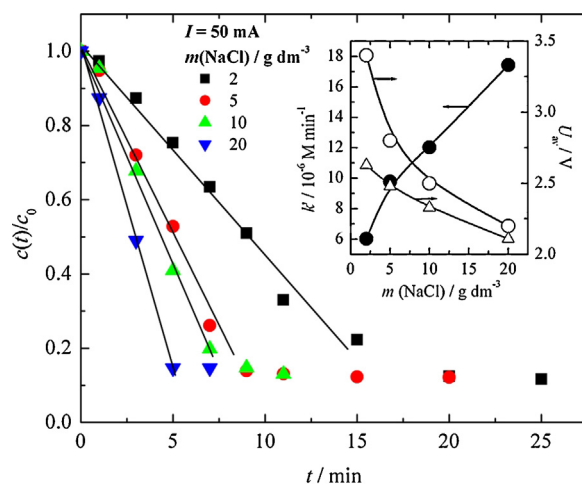| c_0(Meth), mM	k'', min^{-1}	t_t, min	c_t, mM	c_0, %
0.05	0.203	5.1	0.025	50
0.10	0.156	9.63	0.048	48
0.15	0.145	11.0	0.064	42
0.20	0.128	13.6	0.091	43
0.30	0.103	19.6	0.115	38

Fig. 10. Dependence of relative methomyl concentration ($c_0 = 0.1$ mM) over time for different sodium chloride concentration (marked in the figure), $\omega = 325$ rpm. Insert: Dependence of the (●) apparent zero-order reaction rate constant, (○) average and (△) Ohmic drop corrected electrolysis voltage for different NaCl concentration.
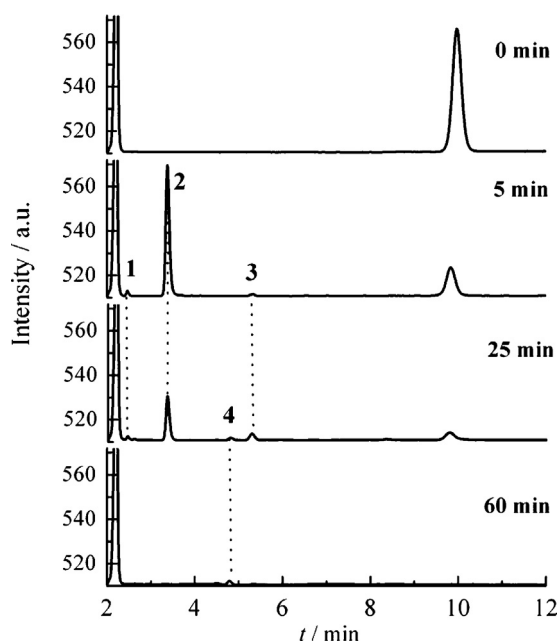
Fig. 11. Typical HPLC chromatograms for four different times of electrolysis under the conditions given in Fig. 4.

linearly increase from 3.89 mS cm^{-1} for 2 g dm^{-3} to 32.8 mS cm^{-1} for 20 g dm^{-3} NaCl using Eq. (7), average electrolysis voltage was corrected for Ohmic drop in the solution, and shown in the insert of Fig. 10. It can be seen that increase in the NaCl concentration from 2 to 5–7 g dm^{-3} can decrease electrolysis voltage loss significantly, from 0.4 to 0.5 V, which will reduce specific energy consumption and increase the reaction rate. So, using the 5 g dm^{-3} NaCl the specific energy consumption will decrease for ~20% and the reaction rate will be faster for ~50%. Higher NaCl concentration will have effect on the Ti/RuO$_2$ anode service life as well.

3.3. HPLC and LC–MS analysis

In order to get more information on the degradation under the conditions applied in this work, we have analyzed the reaction solution using HPLC and LC–MS analyses in positive mode. Typical HPLC chromatograms, obtained under the conditions shown in Fig. 4, for four different times of electrolysis are presented in Fig. 11. After 5 min of the electrolysis, decrease of the methomyl concentration, one main product (peak 2), and some traces of the products (peaks 1 and 3) were observed. For 25 min of electrolysis further decrease of the methomyl concentration and products 2 was observed, as well as appearance of one new unknown trace product denoted with peak 4. Finally, after 60 min of electrolysis, peaks for all products disappeared, except the trace of product 4.

LC–MS (HPLC–ESI-MS) analyses suggested that the main product (peak 2 in Fig. 11) had a molar mass of 178 g mol^{-1} and Bruto formula C$_5$H$_{10}$N$_2$O$_3$S indicating the formation of methomyl sulfoxide (product II in Table 2). An isomer of the same mass was also detected (peak 1 in Fig. 11). This product could be methyl N-hydroxymethylcarbamoyloxyethanimidothioate (product I in

Table 2). Another minor product (peak 3 in Fig. 11), according to LC–MS analysis had a Bruto formula C$_5$H$_{10}$N$_2$O$_4$S and the molar mass of 194 g mol^{-1} (product III in Table 2). This product may be 1-(methylsulfonyl)ethanone O-methylcarbamoyl oxime. After 25 min of the electrolysis another product was detected, namely compound with molar mass of 210 g mol^{-1} and with bruto formula C$_5$H$_{10}$N$_2$O$_5$S (possible: 1-(methylsulfonyl)ethanone O-hydroxymethylcarbamoyl oxime) (product IV in Table 2, not detected in Fig. 11). The formation of products III and IV could be expected since Miles and Oshiro reported the formation of methanesulfonic acid [38].

All detected intermediate products I–III were formed during initial 5 min of the electrolysis. The nature of product with appearance of UV–vis peak at ~251 nm is disputable since all detected intermediates which were formed during the electrolysis higher than five minutes have λ$_{max}$ smaller than 220 nm. Hypothetically, peak at ~251 could be connected with the π–π* transition of the N−C=S group [48,49]. The simplest compounds containing this group could be thioacetamide CH$_3$−C(NH$_2$)=S or its derivates. Thioacetamide has a molar mass of 75.13 g mol^{-1}, and cannot be detected with used LC–MS setup. Since, thioacetamide is suspected B2 carcinogen, if formed degradation can be easily done to sulfate [50] with addition or in situ production of the ferrates in the reaction of μM concentration of iron (III) hydroxide with exes of sodium hypochlorite.

3.4. Possible mechanism of methomyl degradation

Some experimental evidence suggests initial heterogeneous Langmuir–Hinshelwood mechanism, but is elusive, so in the following text we will discuss pro et contra for different possible mechanisms.

Methomyl degradation in the presence of active chlorine species could be considered with three fundamental mechanism: (a) homogeneous (solution) reaction; (b) Eley–Rideal or in this case by the reaction pattern of active chlorine mediated electrochemical incineration of organics proposed by Comninellis [51]; or by (c) heterogeneous Langmuir–Hinshelwood mechanism.

(a) Homogeneous (solution) reaction between most active chlorine species, HOCl, and organic compounds, as elaborated by Deborde and von Gunten [16] and determined for HOCl/OCl$^-$ – methomyl systems [38] the kinetics of the oxidation is second order, i.e., first order in the free active chlorine and first order in the compound concentration:

$$r = kc(\text{HOCl})c(\text{Meth}) \qquad (9)$$

Such reactions are diffusion controlled and reaction rate will increase with increase of the stirring rate, which is not the case in investigated system. One more point is against homogeneous reaction, namely from Fig. 7 it can be seen that 90% of 0.1 mM methomyl at 100 and 200 rpm was degraded within 10 min. Hence, minimum 0.09 mM HOCl should be electrochemically formed. For applied current of 50 mA and taking into account Faraday law, theoretically 0.15 mM of HOCl could be formed. But due to the current efficiency of maximally 20% in low

Table 2
Possible products of electrochemical degradation of methomyl obtained by LC–MS (HPLC–ESI-MS).

No.	Compound	RT[a], min	Exact mass	Ion mass calculated (measured m/z)	λ$_{max}$, nm
I	C$_5$H$_{10}$N$_2$O$_3$S	4.076	178.0412	196.0750 (196.0750); 201.0304 (201.0304)	–
II	C$_5$H$_{10}$N$_2$O$_3$S	4.400	178.0412	196.0750 (196.0750); 201.0304 (201.0303)	204; 214sh
III	C$_5$H$_{10}$N$_2$O$_4$S	4.864	194.0361	195.0434 (195.0436); 212.0699 (212.0696); 217.0253 (217.0252)	204; 212sh
IV	C$_5$H$_{10}$N$_2$O$_5$S	6.765	210.0301	211.0383 (211.0380); 228.0649 (228.0648); 233.0203 (233.0199)	204

[a] Methomyl RT was 6.410 min.

concentration of NaCl [44,47], practically, without dissociation to less active OCl$^-$, only 0.03 mM HOCl will be formed, which is insufficient to oxidize 0.09 mM of methomyl. So, initial rate could not be considered as a homogeneous (solution) reaction.
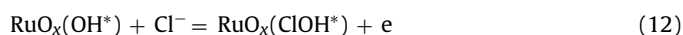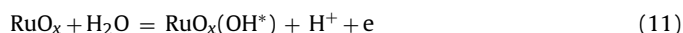
(b) Eley–Rideal mechanism, assumed that an active species (e.g. HOCl*) adsorbed onto electrode oxidize methomyl from solution, and can be given with following rate equation:

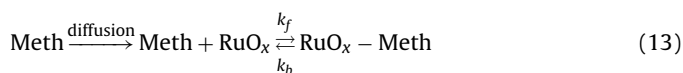$$r = k\theta(ClOH^*)c(Meth) \tag{10}$$

As a consequence, degradation reactions will always follow pseudo-first order kinetics in respect to methomyl [52]. Increase in methomyl concentration will increase reaction rate (as it was observed, see Fig. 8) as well as stirring, diffusion, rate (which was not observed, see insert in Fig. 7). Hence, obtained results practically did not support Eley–Rideal mechanism.

(c) Heterogeneous Langmuir–Hinshelwood mechanism assumed surface chemical reaction between adsorbed species. It is well established that on TiO$_2$ photocatalys degradation of organic pollutant follows Langmuir–Hinshelwood mechanism [5,27]. In the electrochemical waste treatments, adsorption step of some organic compounds was also found on different electrode materials. For example oxalic acid [53], p-methoxyphenol and p-nitrophenol [54,55], or 2,2-dichlorovinyl dimethyl phosphate (dichlorvos) insecticide on SnO$_2$–Sb$_2$O$_5$ electrodes [56].

Obtained experimental observations, as discussed in the above given text, in some manner support the Langmuir-Hinshelwood mechanism. Namely, it has been well established that chloride via electrochemical reaction are adsorbed onto RuO$_2$ surfaces [57]. One of the possible intermediate on RuO$_x$ adsorption site could be chlorohydroxyl radicals (ClOH*) [51,58] which is generated thought following reactions:

$$RuO_x + H_2O = RuO_x(OH^*) + H^+ + e \tag{11}$$

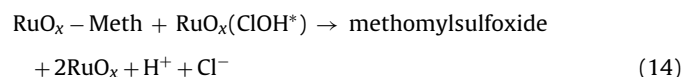$$RuO_x(OH^*) + Cl^- = RuO_x(ClOH^*) + e \tag{12}$$

On the other hand, as observed in the cyclic voltammetry experiments, Fig. 3, adsorption of methomyl onto the unoccupied RuO$_x$ adsorption site, could be also possible:

$$Meth \xrightarrow{diffusion} Meth + RuO_x \underset{k_b}{\overset{k_f}{\rightleftharpoons}} RuO_x - Meth \tag{13}$$

where k_f and k_b are forward and backward methomyl adsorption/desorption rate constants.

At the electrode surface, adsorbed methomyl could react with chlorohydroxyl radicals in the rate determining step, giving initial product II (methomyl sulfoxide):

$$RuO_x - Meth + RuO_x(ClOH^*) \rightarrow methomylsulfoxide$$
$$+ 2RuO_x + H^+ + Cl^- \tag{14}$$

Initially chloride ions are practically not involved in the oxidation, so the reaction pattern of active chlorine mediated electrochemical incineration of organics proposed by Comninellis [50] could be extended in this case on Langmuir-Hinshelwood reaction mechanism.

Since methomyl sulfoxide is an initial product it could be concluded that methomyl was adsorbed onto an electrode with sulfur atoms, which is oxidized by adsorbed chlorohydroxyl radicals producing =S=O group.

Hence, if an oxidation rate is much lower than the diffusion and adsorption rate, the overall rate equation may be written as:

$$r = -\frac{\partial c(Meth)}{\partial t} = k\theta(ClOH^*)\theta(Meth) \tag{15}$$

where k is the oxidation rate constant, $\theta(Meth)$ the fractional surface coverage of methomyl and $\theta(ClOH^*)$ is the fractional surface coverage of the chlorohydroxyl radical. If assumed that methomyl was adsorption under Langmuir conditions, $\theta(Meth)$ may be represented as:

$$\theta(Meth) = \frac{Kc(Meth)}{1 + Kc(Meth)} \tag{16}$$

where

$$K = \frac{k_f}{k_b} \tag{17}$$

is methomyl adsorption/desorption equilibrium constant. In the first approximation, $\theta(ClOH^*)$ could not be expressed in terms of a Langmuir isotherm since does not correspond to an adsorption–desorption equilibrium. However, it may consider that its value remains constant for the same current and concentration of sodium chloride. Thus, for such conditions the overall rate equation can be written as:

$$r = -\frac{\partial c(Meth)}{\partial t} = k\theta(ClOH^*)\frac{Kc(Meth)}{1 + Kc(Meth)} = k'\frac{Kc(Meth)}{1 + Kc(Meth)} \tag{18}$$

where k' is the apparent heterogeneous oxidation rate constant.

For conditions that $Kc(Meth) \gg 1$, Eq. (18) is transformed in $r = k''$, giving the pseudo zero reaction rate expressed as:

$$\frac{c(t)}{c_0} = 1 - \frac{k'}{c_0}t \tag{19}$$

and for conditions that $Kc(Meth) \ll 1$, Eq. (18) is transformed in $r = k'Kc(Meth) \sim k''c(Meth)$ giving the pseudo first reaction rate, expressed as:

$$\ln\frac{c(t)}{c_0} = -k''t \tag{20}$$

Obtained initial zero-order rate and transition to first order are in agreement with given discussion. Hence, in the whole range of concentrations more complex equation should be applied as suggested by Kumar [59]:

$$-\ln\left(\frac{c(t)}{c_0}\right) - K[c(t) - c_0] = k_{app}Kt \tag{21}$$

Considering the polarization data given in Fig. 3, a few valuable information can be obtained. Following the same assumption of the Langmuir–Hinshelwood reaction mechanism, the current density can be expressed as:

$$j = nFk_{ox}(E)\theta(ClOH^*)\theta(Meth) \tag{22}$$

where $k_{ox}(E)$ is a potential dependent oxidation rate constant. For the constant potential, $\theta(ClOH^*)$ could be considered constant, as well and the surface coverage of the methomyl can be given as:

$$\theta(Meth) = \left[\frac{j - j_{(Meth=0)}}{j}\right]_{E=const} \tag{23}$$

Using Eq. (23) and values of the current densities shown in the insert of Fig. 12, the dependence of the methomyl surface coverage on the concentration for different constant potentials can be estimated as shown in Fig. 12. The typical Langmuir adsorption isotherm was obtained, and surface coverage of the methomyl increase with the increase of the bulk methomyl concentration, reaching maximum of 0.55–0.65 depending on the applied potential. The methomyl concentration coverage decrease with electrode potential, which is in agreement with faster rate of electrochemical formation of chlorohydroxyl radicals.

Using the obtained data for the dependence of surface coverage on methomyl concentration the methomyl adsorption/desorption
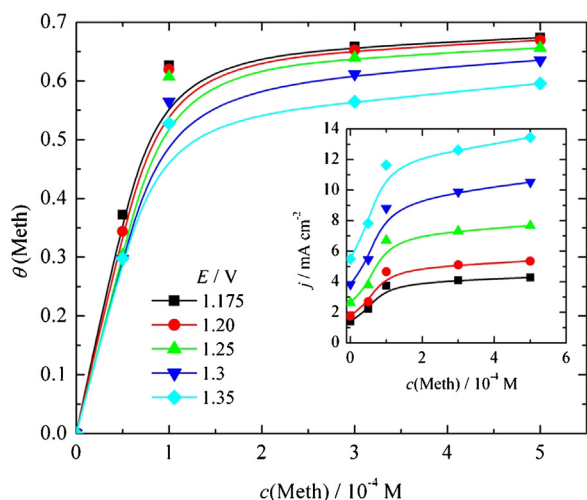
Fig. 12. Dependence of the methomyl surface coverage on the bulk concentration for different constant potentials. Insert: dependence of the current density on methomyl concentration for different constant potentials, evaluated from Fig. 3.

equilibrium constant, K, can be estimated using a modified form of Eq. (16):

$$\frac{c(\text{Meth})}{\theta_E(\text{Meth})} = \frac{1}{K} + c(\text{Meth}) \tag{24}$$

Another method can be applied to estimate graphically K and saturation value of k'_{sat} using a linearized form of Eq. (18)

$$-\frac{1}{r_0} = \frac{1}{k'_{sat}} + \frac{1}{k'_{sat} K c(\text{Meth})} \tag{25}$$

where $-1/r_0$ is plotted against $1/c$. The value of r_0 was essentially the same as k' taking into account Eq. (19) and Fig. 8. From the graphical presentation of Eqs. (24) and (25) shown in Fig. 13, the value of methomyl adsorption/desorption equilibrium constant was roughly estimated to be $K = (1.8 \pm 0.3) \times 10^4 \, \text{M}^{-1}$, and the saturation apparent zero reaction rate constant $k'_{sat} \sim 1 \times 10^{-5} \, \text{M min}^{-1}$. Using this initial values, the experimental dependence of k' on c_0 shown in the insert of Fig. 8 was fitted using Eq. (18), and the values of $K = 17.9 \times 10^3 \, \text{M}^{-1}$ and $k'_{sat} = 1.09 \times 10^{-5} \, \text{M min}^{-1}$ was obtained, and shown as solid curve in the insert of Fig. 8. Considering that in the investigated ranges of the concentrations we assumed that $k'_{sat} \times K \approx k''$, so the average value of k'' of 0.155 min^{-1}, are in good agreement with $k'_{sat} \times K$ of 0.195 min^{-1} which further support the proposed mechanism.
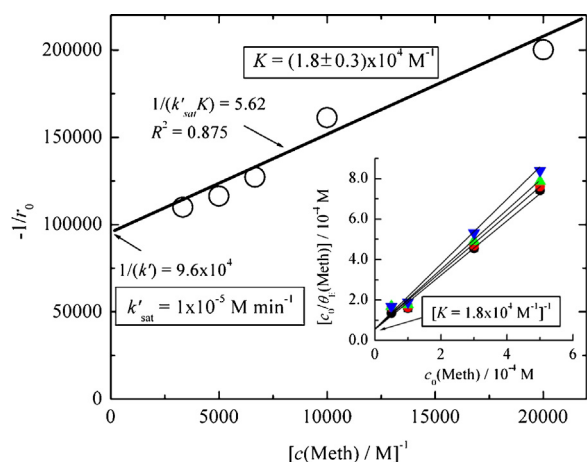

Fig. 13. Graphical presentation of Eq. (25). Insert: graphical presentation of Eq. (24).
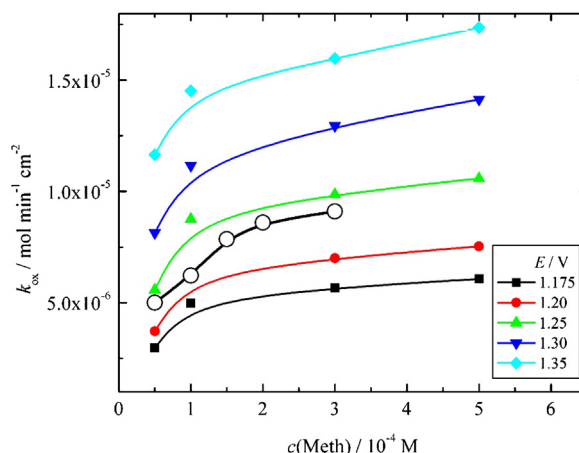

Fig. 14. Dependence of the estimated apparent zero reaction rate constant on methomyl concentration from polarization measurements (full symbols Eq. (26), –○– UV–vis data).

It should be noted that parallel with given Langmuir–Hinshelwood reaction mechanism, formation of "active chlorine species" could occur as well, especially after prolonged electrolysis, which can further react with product II or methomyl in solution *via* homogenous reaction giving other trace products.

The value of K is related to the standard free energy of adsorption, ΔG^θ, with the following equation [60]:

$$K = \frac{1}{55.5} \exp\left(-\frac{\Delta G^\theta}{RT}\right) \tag{26}$$

where the value 55.5 is the concentration of water in solution (mol dm^{-3}), R gas constant (8.314 J mol^{-1} K^{-1}), T thermodynamic temperature (298.15 K), and the standard free energy of $\Delta G^\theta = -34.3 \, \text{kJ mol}^{-1}$ can be calculated. The negative values of ΔG^θ ensure the spontaneity of the adsorption process and stability of the adsorbed methomyl on the RuO$_2$ surface. Generally, values of ΔG^θ around $-20 \, \text{kJ mol}^{-1}$ or higher are consistent with the electrostatic interaction between the charged molecules and the charged metal (physisorption) [60]. On the other hand Ferro and De Battisti [57] reported the value of $K(\text{Cl}^-) = \sim 0.4 \, \text{M}^{-1}$ in 0.01 M perchloric acid and 0.1–2 M sodium chloride on RuO$_2$ deposited on conductive diamond electrode. So, competitive adsorption of methomyl and Cl$^-$ could occur in the investigated system.

Modified Eq. (22) and taking data from Fig. 12 can be used to estimate the apparent zero reaction rate constant from polarization measurements:

$$k_{ox}(E) = \frac{j_{E=\text{const}}}{nF\theta(\text{ClOH}^*)\theta(\text{Meth})} \tag{27}$$

For the calculations, the numbers of exchanged electrons for the overall reaction $n = 2$, units of Faraday constant F are expressed in A min mol^{-1}, with approximation that $\theta(\text{ClOH}^*) \approx 1 - \theta(\text{Meth})$, were used. The apparent zero reaction rate constant at different constant potentials are calculated and shown in Fig. 14. Comparing this data with ones obtained from UV measurements relatively good accordance was obtained from the anode potential of $\sim$1.25 V. This potential is in a good agreement whit that obtained from the polarization measurements (see Fig. 3), suggesting that both electrochemical and nonelectrochemical techniques could be successfully used for investigation of the pesticide degradation.

4. Conclusions

Electrochemical degradation of the methomyl in chloride containing solutions on DSA Ti/RuO$_2$ electrode was

investigated by the means of electrochemical techniques, UV–vis spectrofotometry, HPLC and HPLC–ESI-MS. It was concluded that initially methomyl degradation follows heterogeneous Langmuir–Hinshelwood pseudo zero-order mechanism, where adsorbed intermediates are chlorohydroxyl radical (ClOH*) and methomyl adsorbed with sulfur atoms onto catalyst surface. After prolonged electrolysis transition from initial zero to first-order reaction was observed. It was also concluded that Cl$^-$ mediated oxidation of organic substrates could be extended on Langmuir–Hinshelwood mechanism. Reaction rate of methomyl degradation increase with applied current and sodium chloride concentration, and with lower mixing rate. Analyzing the specific energy consumption it was concluded that optimum electrolysis condition should be with current density of ~10–20 mA cm^{-2} in solution containing ~5 g dm^{-3} NaCl with minimum stirring. Under such conditions ~90% of methomyl will degrade within 0.5 h which is comparable with AOPs processes. As the main reaction intermediate of the electrochemical degradation, methomyl sulfoxide was suggested, which could further react in homogenous reaction with "active chlorine species". Using the mathematical treatment the value of methomyl adsorption/desorption equilibrium constant of $K = 17.9 \times 10^3$ M^{-1}, and the saturation apparent zero-order reaction rate constant $k'_{sat} = 1.09 \times 10^{-5}$ M min^{-1} was estimated. Apparent pseudo first-order rate constant was determined to be ~0.1–0.2 min^{-1}.

Acknowledgement

References

[1] C.A. Martínez-Huitle, S. Ferro, Chem. Soc. Rev. 35 (2006) 1324–1340.
[2] A.R. Van Scoy, M. Yue, X. Deng, R.S. Tjeerdema, Rev. Environ. Contam. Toxicol. 222 (2013) 93–109.
[3] S. Malato, J. Blanco, C. Richter, M.I. Maldonado, Appl. Catal. B 25 (2000) 31–38.
[4] S. Malato, J. Blanco, J. Cáceres, A.R. Fernández-Alba, A. Agüera, A. Rodríguez, Catal. Today 76 (2002) 209–220.
[5] M.A. Quiroz, E.R. Bandala, C.A. Martínez-Huitle, in: M. Stoytcheva (Ed.), Pesticides—Formulations, Effects, Fate, InTech, Rijeka, Croatia, 2013, pp. 685–730.
[6] F.C. Moreira, S. Garcia-Segura, V.J.P. Vilar, R.A.R. Boaventura, E. Brillas, Appl. Catal. B 142–143 (2013) 877–890.
[7] E. Brillas, I. Sirés, M.A. Oturan, Chem. Rev. 109 (2009) 6570–6631.
[8] N. Oturan, I. Sirés, M.A. Oturan, E. Brillas, J. Environ. Eng. Manage. 19 (2009) 235–255.
[9] C.A. Martínez-Huitle, A. De Battisti, S. Ferro, S. Reyna, M. Cerro-López, M.A. Quiro, Environ. Sci. Technol. 42 (2008) 6929–6935.
[10] A. Kraft, M. Stadelmann, M. Blaschke, D. Kreysig, B. Sandt, F. Schroéder, J. Rennau, J. Appl. Electrochem. 29 (1999) 861–868.
[11] C.A. Martínez-Huitle, E. Brillas, Appl. Catal. B 87 (2009) 105–145.
[12] G. Chen, Sep. Purif. Technol. 38 (2004) 11–41.
[13] A. Vlyssides, D. Arapoglou, S. Mai, E.M. Barampouti, Chemosphere 58 (2005) 439–447.
[14] J. Muff, C.D. Andersen, R. Erichsen, E.G. Soegaard, Electrochim. Acta 54 (2009) 2062–2068.
[15] S.E. Duirk, T.W. Collette, Organophosphate pesticide degradation under drinking water treatment conditions, U.S. Environmental Protection Agency, Washington, DC, EPA/600/R-05/103 (NTIS PB2006-101091), 2005, pp. 2.
[16] M. Deborde, U. von Gunten, Water Res. 42 (2008) 13–51.
[17] A. Lopez, G. Mascolo, G. Tiravanti, M. Santori, R. Passino, Water Sci. Technol. 30 (1994) 53–59.
[18] G. Mascolo, A. Lopez, R. Passino, G. Ricco, G. Tiravanti, Water Res. 28 (1994) 2499–2506.
[19] C.J. Miles, Environ. Sci. Technol. 25 (1991) 1774–1779.
[20] Y.Z. Mason, E. Choshen, C. Ravacha, Water Res. 24 (1990) 11–21.
[21] S. Kodama, A. Yamamoto, A. Matsunaga, J. Agric. Food. Chem. 45 (1997) 990–994.
[22] W.J. Hayes, E.R. Laws (Eds.), Handbook of Pesticide Toxicology, Classes of Pesticides, vol. 3, Academic Press, Inc., New York, 1990.
[23] C.D.S. Tomlin, The Pesticide Manual, 15th ed., BCPC Publications, 2009, pp. 757.
[24] T.J. Strathmann, A.T. Stone, Environ. Sci. Technol. 35 (2001) 2461–2469.
[25] EFSA, Conclusion on Pesticide Peer Review Regarding the Risk Assessment of the Active Substance Methomyl, European Food Safety Authority (EFSA). EFSA Scientific Report 222, 2008, pp. 1–99.
[26] C. Jansson, T. Pihlström, B.-G. Österdahla, K.E. Markides, J. Chromatogr. A 1023 (2004) 93–104.
[27] M. Tamimi, S. Qourzal, A. Assabbane, J.-M. Chovelon, C. Ferronato, Y. Ait-Ichou, Photochem. Photobiol. Sci. 5 (2006) 477–482.
[28] M. Tamimi, S. Qourzal, N. Barka, A. Assabbane, Y. Ait-Ichou, Sep. Purif. Technol. 61 (2008) 103–108.
[29] S. Malato, J. Blanco, A. Vidal, D. Alarcóon, M.I. Maldonado, J. Cáceres, W. Gernjak, Sol. Energy 75 (2003) 329–336.
[30] I. Oller, W. Gernjak, M.I. Maldonado, L.A. Pérez-Estrada, J.A. Sánchez-Pérez, S. Malato, J. Hazard. Mater. 138 (2006) 507–517.
[31] N.A.M. Barakat, M.M. Nassar, T.E. Farrag, M.S. Mahmoud, Environ. Sci. Pollut. Res. (2013), in press
[32] A. Tomašević, G. Bošković, D. Mijin, E.E. Kiss, React. Kinet. Catal. Lett. 91 (2007) 53–59.
[33] A. Tomašević, S. Petrović, E. Kiss, D. Mijin, Desalination 262 (2010) 228–234.
[34] A. Tomašević, D. Mijin, E. Kiss, Sep. Sci. Technol. 45 (2010) 1617–1627.
[35] M.M. Mico, S. Chourdaki, J. Bacardit, C. Sans, Ozone – Sci. Eng. 32 (2010) 259–264.
[36] M.M. Micó, J. Bacardit, J. Malfeito, C. Sans, Appl. Catal. B 132–133 (2013) 162–169.
[37] E. Chamberlain, H. Shi, T. Wang, Y. Ma, A. Fulmer, C. Adams, J. Agric. Food Chem. 60 (2012) 354–363.
[38] C.J. Miles, W.C. Oshiro, Environ. Toxicol. Chem. 9 (1990) 535–540.
[39] A.V. Tomašević, M.L. Avramov-Ivić, S.D. Petrović, M.B. Jovanović, D.Ž. Mijin, J. Serb. Chem. Soc 74 (2009) 573–579.
[40] N. Oturan, M.A. Oturan, Agron. Sustain. Dev. 25 (2005) 267–270.
[41] N. Oturan, M. Zhou, M.A. Oturan, J. Phys. Chem. A 114 (2010) 10605–10611.
[42] A. Kesraoui Abdessalem, N. Bellakhal, N. Oturan, M. Dachraoui, M.A. Oturan, Desalination 250 (2010) 450–455.
[43] I.S. Park, Y.Y.J. Tong, Electrocatalysis 4 (2013) 117–122.
[44] S. Neodo, D. Rosestolato, S. Ferro, A. De Battisti, Electrochim. Acta 80 (2012) 282–291.
[45] L.C. Adam, I. Fábián, K. Suzuki, G. Gordon, Inorg. Chem. 31 (1992) 3534–3541.
[46] R. Vargasa, C. Borrása, J. Mostanya, B.R. Scharifker, Electrochim. Acta 80 (2012) 326–333.
[47] F. Zaviska, P. Drogui, J-F. Blais, G. Mercier, J. Appl. Electrochem. 39 (2009) 2397–2408.
[48] L. Liu, J. Wu, X. Li, Y. Ling, Sep. Purif. Technol. 103 (2013) 92–100.
[49] A.G. Dodge, J.E. Richman, G. Johnson, L.P. Wackett, Appl. Environ. Microbiol. 72 (2006) 7468–7476.
[50] V.K. Sharma, R.A. Rendon, F.J. Millero, F.G. Vazquez, Mar. Chem. 70 (2000) 235–242.
[51] Ch. Comninellis, Electrochim. Acta 39 (1994) 1857–1862.
[52] D.C. Johnson, J. Feng, L.L. Houk, Electrochim. Acta 46 (2000) 323–330.
[53] S. Ferro, C.A. Martínez-Huitle, A. De Battisti, J. Appl. Electrochem. 40 (2010) 1779–1787.
[54] R. Vargas, C. Borras, D. Plana, J. Mostany, B.R. Scharifker, Electrochim. Acta 55 (2010) 6501–6506.
[55] C. Borras, C. Berzoy, J. Mostany, J.C. Herrera, B.R. Scharifker, Appl. Catal. B 72 (2007) 98–104.
[56] R.S. Díaza, L. Vieleb, O. Núñezb, C. Borrása, J. Mostanya, B.R. Scharifkera, Appl. Catal. B 144 (2014) 107–111.
[57] S. Ferro, A. De Battisti, J. Phys. Chem. B 106 (2002) 2249–2254.
[58] F. Bonfatti, S. Ferro, F. Lavezzo, M. Malacarne, G. Lodi, A. De Battisti, J. Electrochem. Soc. 147 (2000) 592–596.
[59] K. Porkodi, K.V. Kumar, Appl. Catal. B 79 (2008) 108–109.
[60] Q.-Q. Liao, Z.-W. Yue, D. Yang, Z.-H. Wang, Z.-H. Li, H.-H. Ge, Y.-J. Li, Thin Solid Films 519 (2011) 6492–6498.